Hybrid Inorganic−Organic Adsorbents Part 1: Synthesis and Characterization of Mesoporous Zirconium Titanate Frameworks Containing Coordinating Organic Functionalities

Christopher S. Griffith,[†] Massey De Los Reyes,[‡] Nicholas Scales,[‡] John V. Hanna,[§] and Vittorio Luca*,[⊥]

Institute of Materials Engineering and ANSTO Minerals, Australian Nuclear Science and Technology Organisation, Locked Bag 2001, Kirrawee DC, New South Wales 2232, Australia, Comisión Nacional de Energía Atómica, Centro Atómico Constituyentes, Avenida General Paz 1499, 1650 San Martin, Provincia de Buenos Aires, Argentina, and Department of Physics, University of Warwick, Gibbet Hill Road, Coventry CV4 7AL, United Kingdom

ABSTRACT A series of functional hybrid inorganic−organic adsorbent materials have been prepared through postsynthetic grafting of mesoporous zirconium titanate xerogel powders using a range of synthesized and commercial mono-, bis-, and tris-phosphonic acids, many of which have never before been investigated for the preparation of hybrid phases. The hybrid materials have been characterized using thermogravimetric analysis, diffuse reflectance infrared (DRIFT) and ^{31}P MAS NMR spectroscopic techniques and their adsorption properties studied using a ^{153}Gd radiotracer. The highest level of surface functionalization (molecules/nm^2) was observed for methylphosphonic acid (~3 molecules/nm^2). The level of functionalization decreased with an increase in the number of potential surface coordinating groups of the phosphonic acids. Spectral decomposition of the DRIFT and ^{31}P MAS NMR spectra showed that each of the phosphonic acid molecules coordinated strongly to the metal oxide surface but that for the 1,1-bis-phosphonic acids and tris-phosphonic acids the coordination was highly variable resulting in a proportion of free or loosely coordinated phosphonic acid groups. Functionalization of a porous mixed metal oxide framework with the tris-methylenephosphonic acid (**ATMP**-ZrTi-0.33) resulted in a hybrid with the highest affinity for $^{153}Gd^{3+}$ in nitric acid solutions across a wide range of acid concentrations. The **ATMP**-ZrTi-0.33 hybrid material extracted $^{153}Gd^{3+}$ with a K_d value of 1×10^4 in 0.01 M HNO$_3$ far exceeding that of the other hybrid phases. The unfunctionalized mesoporous mixed metal oxide had negligible affinity for Gd^{3+} ($K_d < 100$) under identical experimental conditions. It has been shown that the presence of free or loosely coordinated phosphonic acid groups does not necessarily translate to affinity for $^{153}Gd^{3+}$. The theoretical cation exchange capacity of the **ATMP**-ZrTi-0.33 hybrid phase for Gd^{3+} has been determined to be about 0.005 mmol/g in 0.01 M HNO$_3$. This behavior and that of the other hybrid phases suggests that the surface-bound **ATMP** ligand functions as a chelating ligand toward $^{153}Gd^{3+}$ under these acidic conditions.

KEYWORDS: hybrid inorganic−organic • mesoporous zirconium titanate • adsorbent • isotope

1. INTRODUCTION

The synthesis of porous metal oxides that possess functional organic molecules grafted to the internal pore walls has been a very active area of research over past decades (1−7). These types of materials have extremely diverse potential applications, such as in the fields of separation, catalysis, drug release, and sensors. Although the vast majority of work has been conducted using siliceous mesoporous frameworks, recent interest has been directed toward nonsiliceous materials. Particular interest has been paid to metal oxide frameworks, especially titanium-based

materials, as these offer significant diversity with respect to their chemical, electronic and optical properties. Arguably the improved synthetic routes (with respect to those of siliceous materials) for metal oxide frameworks with well-defined porosity and topology has fuelled the interest in these materials. One of our group's principal interests in this area is the development and study of mesoporous and supermicroporous metal oxide materials functionalized with organic moieties for the selective separation of aqueous metal species, particular radioactive species. Indeed, such functional materials can show considerable promise for the adsorption of heavy metal species (8, 9).

In principle, the design and synthesis of any functionalized porous material involves consideration of: (1) the application conditions; (2) the porous framework; (3) the "anchor" group; and (4) the required "free" functional unit (Figure 1). With respect to (1), irradiated nuclear fuel reprocessing flow sheets are usually associated with moderate to highly acidic aqueous media. Hence, acid-stable support frameworks, anchors, and functional groups are required for
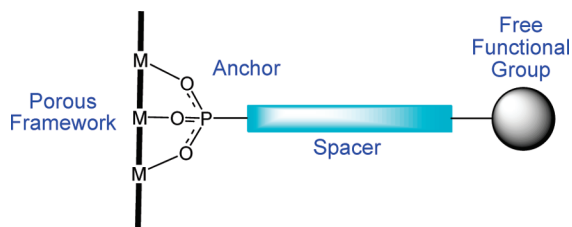
FIGURE 1. Schematic description of a functionalized pore surface highlighting the key factors: framework, anchor group, spacer, and pendent coordinating group.

ATMP   **PIDC**   **HEDP**

HABDP   **BuDP**   **BenDP**

FIGURE 2. Range of phosphonic acids investigated for their ability to functionalized the mesoporous phase, ZrTi-0.33.

hybrid materials targeted for this application. In relation to (2), the choice of an appropriate supporting framework is an issue that has itself a number of further considerations such as effective surface area, physical form (powdered or granular), and hydrolytic and radiolytic stability (in a nuclear context). Under mildly acidic conditions, siliceous phases are applicable; however, hydrolytic stability is a concern (10). The application of porous metal oxide adsorbents, particularly those based on the Group IV metals, zirconium and titanium, offer the prospect of ready conversion of the "spent" adsorbent containing adsorbed radiogenic species to a highly durable ceramic rather than a less stable glass. We have recently validated the potential of this approach by demonstrating that Ca^{2+}-impregnated mesoporous zirconium titanate could be converted to the highly durable ceramic, zirconolite, at temperatures as low as 900 °C (11). We have modified the precursor chemistry of this system so as to allow access to almost super microporous powdered phases (12), as well as millimeter-sized beads containing mesoporosity and/or macroporosity (13). With the present nuclear application in mind, it is advantageous to have the flexibility to adjust the framework composition from one that is titanium rich to one that is zirconium rich, and in so doing, modify the properties of the metal oxide framework and of the crystalline ceramics formed on heating. Although we have already demonstrated that it is possible to prepare mixed zirconium titanium oxides with comparable porosity and mesoporous texture in bead form, a fixed composition $(Zr_{0.33}Ti_{0.66}O_2)$ was chosen for the present study.

The hydrolytic stability of M−O−P bonds is well-known as evidenced by the vast array of metal phosphate chemistry reported over the last three decades (14). Hence, this provides a starting point in addressing item (3). There has also been significant interest in employing phosphonate linkages in place of carboxylates for dye-sensitized solar cell applications (15−18). Early interest in employing phosphonic acid anchor groups with Group IV oxides for other applications came from the groups of Mallouk (19) and Katz (20) where multilayer zirconate layers were sequentially deposited on gold substrates. Modification of other planar substrates such as Indium Tin Oxide (ITO) electrodes (21), titanium foil (22, 23), and titania/zirconia-coated glass (24) followed this earlier work. The first report of investigations on bulk powdered phases was from Reven and co-workers who demonstrated the affinity of simple alkyl phosphonic acids for bulk titania (Degussa P25) and zirconia (Deg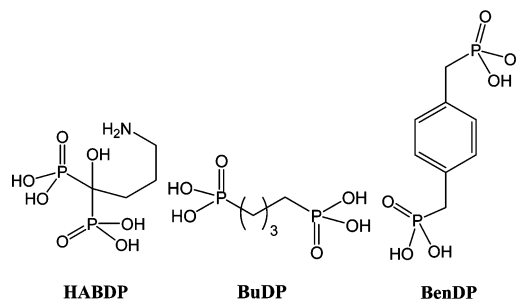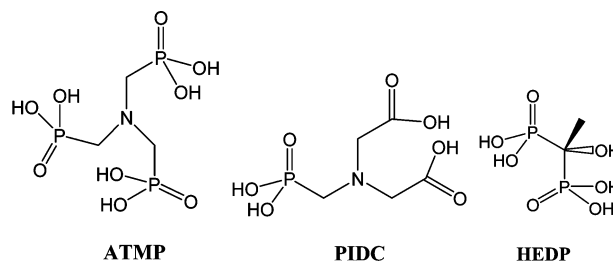ussa AG). It was also shown that the adsorbed monolayers possessed conformational order comparable to self-assembled monolayers on planar substrates (25). These investigators also reported the coordination behavior of variable alkyl chain length molecules terminated by phosphonic and carboxylic acids $H_2O_3P(CH_2CH_2)_xCO_2H$ ($x = 2-15$) on similar bulk phases. For both titanate and zirconate xerogel powders, anchoring was found to predominately occur via the phosphonic acid moiety, although for short chain lengths ($x = 2$ and 3), some anchoring via the carboxylic acid was observed for the titanate phase. Fadeev and co-workers (26) have explored the coordination of alkyl phosphonic acid, silane and chlorosilane molecules on titania and zirconia in a number of reports, demonstrating the stability of the phosphonate anchor across a broad range of pH. Since early 2001, Mutin and co-workers have reported on the potential of employing a phosphate anchor group for the preparation of organic−inorganic hybrid titanate-based phases using primarily sol−gel synthetic routes. However, in one of their initial reports (27), they showed that the coordination of phenyl phosphonic acids, esters and silyl ethers to titania (Degussa P25) appeared to occur via a tridentate bonding mode and that coupling occurs at both the surface hydroxyls and Lewis acid sites. Subsequent ^{17}O Solid State NMR (SS-NMR) investigations unequivocally proved that the tridentate coordination mode was the predominate surface species for this aryl phosphonic acid (28). Given the large range of pendent functional groups possible with respect to point (**4**), in this study we have limited potential coordinating groups to that of phosphonic, carboxylic, and amino functional groups. However, subsequent studies are aimed at actinide-specific coordinating groups.

The aim of the present body of investigation was to functionalize a well-studied (11−13) mesoporous zirconium titanate framework with wormhole morphology, using a series of simple mono-, bis-, and tris-phosphonic acids (Figure 2) to produce novel hybrid inorganic−organic ma-

Scheme 1. Simplified Reaction Scheme for the Synthesis of the Noncommercial Bis-phosphonic Acids, BuDP and BenDP
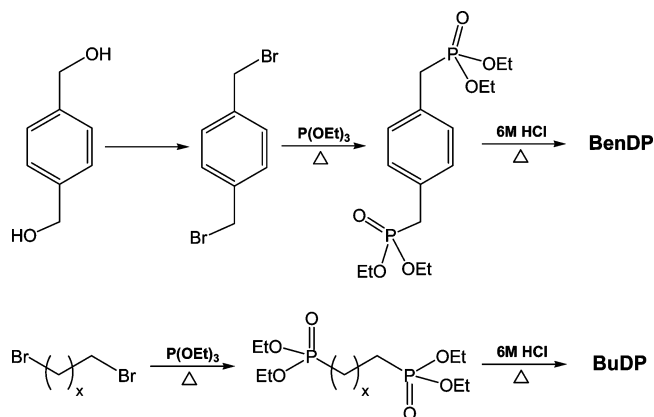
terials. Moreover, our investigations were aimed at identifying any systematic variations in adsorption properties and to evaluate the utility of these hybrid materials as lanthanide and minor actinide adsorbents within the context of advanced nuclear fuel recycling. This has been undertaken using [153]Gd radiotracers as probes of the structure−function relationships of these materials. The coordination of the phosphonic acids to the pore surfaces has been elucidated using diffuse reflectance infrared spectroscopy (DRIFT), solid-state ^{31}P MAS NMR, and thermogravimetric techniques.

2. EXPERIMENTAL SECTION

General. Analytical grade reagents and solvents (of at least >99% purity) from Sigma Aldrich were employed for the syntheses of the noncommercial phosphonic acids and mesoporous zirconium titanate phase. Synthesis of the precursor alkyl and aryl bromo and corresponding phosphonates were conducted using standard Schlenk techniques under nitrogen. The phosphonic acids methylphosphonic acid (**MeP**), amino tris-methylenephosphonic acid (**ATMP**), phosphono-imido-dicarboxylic acid (**PIDC**), 4-amino,1-hydroxy,1,1-bis-phosphonic acid butane (**HABDP**), and 1-hydroxylethylene-1,1-bis-phosphonic acid (**HEDP**) were sourced from Aldrich as hygroscopic solids or as an aqueous solution (**ATMP**, 50% w/w) and were used as received. The noncommercial bis-phosphonic acids, 1,4-diphosphonic acid butane (**BuDP**) and 1,4-diphosphonic acid benzene (**BenDP**), were synthesized via Michaels−Arbuzov addition of P(OEt)$_3$ to the corresponding bromo-derivatives, followed by hydrolysis using hydrochloric acid (Scheme 1) (29). The bromo, phosphonate esters, and phosphonic acids were all characterized by multinuclear NMR (^{1}H, ^{13}C, and ^{31}P) and FT-IR spectroscopy and used without further purification.

Thermogravimetric analysis (TGA) and differential thermal analysis (DTA) were conducted simultaneously on a Setaram TAG24 (France) with high purity instrument air as the carrier gas. Before analysis, the parent and functionalized mesoporous phases were dried (50 °C, 10 mmHg, 12−14 h) to remove most of the physi-sorbed water so as to enable an accurate determination of the temperature at which the functionalized organic molecule was thermalized from the mesoporous phase. Calculation of the degree of functionalization has been expressed as the number of organic molecules (Phos) per nm^2. The surface area of the mesoporous zirconium titanate phases were determined using nitrogen gas adsorption on a Micromeritics ASAP 2010 instrument using the BET method.

Diffuse reflectance FT-IR (DRIFT) of the dried parent and functionalized mesoporous phases were recorded in KBr (5%

w/w) in the range 4000−650 cm^{-1} with a Nicolet Nexus 8700 FT-IR spectrometer equipped with a liquid nitrogen-cooled HgCdTe detector and a ThermoElectron Diffuse Reflectance (DRIFT) accessory. Decomposition of the spectra using the GRAMS32 software suite followed subtraction of the DRIFT spectra of the parent zirconium titanate phase.

Phosphorus-31 solid-state magic angle spinning (MAS) nuclear magnetic resonance (NMR) data were acquired at ambient temperature on a Bruker MSL-400 spectrometer operating at a ^{31}P frequency of 161.92 MHz. Conventional single-pulse (Bloch decay) experiments with high-power ^{1}H decoupling during acquisition and cross-polarization experiments were implemented on a Bruker 4 mm double-air-bearing probe utilizing MAS frequencies of ∼10 kHz. The single-pulse experiments used $\pi/4$ excitation pulses with recycle delays of 20s. For the cross-polarization measurements, an initial [1]H $\pi/2$ pulse of 3 μs, a Hartmann−Hahn contact period of 10 ms and a recycle delay of 10 s were common to all measurements. All ^{31}P chemical shifts were measured with respect to 85% H$_3$PO$_4$ via an external sample of (NH$_4$)H$_2$(PO$_4$), which was also used to establish the Hartmann−Hahn match condition.

Synthesis of Mesoporous Titanate Zirconate (ZrTi-x). The mesoporous zirconium titanate phase (ZrTi-x) employed in this study was synthesized using a slight modification of the preparation reported previously by our group (11). To a stirred mixture of zirconium propoxide (70% w/w in propanol) and titanium isopropoxide (x = Zr/Zr + Ti molar ratio = 0.33) was added palmitic acid in a nitrogen filled drybox. The amount of carboxylate surfactant added was calculated to afford a Metal: Surfactant ratio equal to 2. The mixture was then heated at 70 °C with stirring until a homogeneous mixture was obtained. After cooling to ambient temperature, the mixture was transferred to a Pyrex drying tray then incubated in a reactor system in which air humidified at 70−80% RH was passed over the precursor solution at constant flow (*ca*. 900 mL min^{-1}) and constant temperature (35 °C). Once the reaction mixture had gelled and become opaque, excess deionized water was added and the resulting coarse, colorless solid filtered, washed with deionized water and dried at 70 °C. Removal of the surfactant template was undertaken by thermal treatment at 450 °C for 7 h in air. The ZrTi-0.33 phase prepared by this method displayed a single low angle X-ray correlation peak at ca. 3.5 nm (Scintag X1 X-ray diffractometer, 1.524 Å Cu K_α) and BET surface area of 245 m^2 g^{-1} and a narrow pore size distribution centered at 3.57 nm as determined using non-localized density functional theory (NL-DFT). This was consistent with our previous report on such materials, and hence, the material was used without further characterization.

Functionalization of Zirconium Titanate Mesoporous (P-ZrTi-0.33) Phase. Functionalization was typically undertaken by contacting a portion of ZrTi-0.33 (1 g) with a solution (41 mM) of the appropriate phosphonic acid for 12 h in a sealed vessel. The pH of the mixture was not adjusted. The solid was then filtered, washed with deionized water (18.2 MΩ) until the filtrate was neutral, and then a small volume of ethanol. Finally, the solid was dried at 70 °C for 12 h, and then in vacuo (10 mmHg, 50 °C) for 12 h.

Ion-Exchange Investigations−Radiochemical and Elemental Analysis. The ion-exchange properties of the parent (ZrTi-0.33) and functionalized (**P**-ZrTi-0.33) phases were investigated in triplicate using the batch contact method. For the radiochemical investigations, contact experiments were conducted in the absence of inactive carrier, where the powdered sorbent (50 ± 1 mg) and a given nitric acid solution (0.00001−3 M; 4 mL) containing approximately 1 000 000 cpm of [153]Gd (>99% purity; Perkin-Elmer Life Sciences) were contacted at 25 °C for 30 min with agitation in a standard glass Kimble tube (5 mL). After a given contact time, the reaction mixtures were centrifuged (5000 rpm, 7 min.) and three separate 1 mL aliquots of each

supernatant removed for analysis. Triplicate samples of the initial ^{153}Gd activity and triplicate samples of the individual contact experiments were counted for 20 s on an automated Wallac 1480 Wizard 3" gamma counter using a wide energy window. The activity of the initial solutions and final supernatants were taken as the average of the triplicate analyses and the respective errors calculated using the range of the three analyses. The determination of the radionuclide activity before and after contact with a given adsorbent allowed the calculation of a distribution coefficient (K_d) for the given metal cation with respect to the adsorbent by eq 1

$$K_{\mathrm{d}} = \frac{(A_{\mathrm{i}} - A_{\mathrm{f}})}{A_{\mathrm{f}}} \frac{V}{m} \frac{1}{F} \tag{1}$$

where A_{i} = initial radiotracer activity; A_{f} = final radiotracer activity; V = volume of solution contacted with adsorbent; m = mass of adsorbent employed; F = form factor (%) to normalize for hydration of the given adsorbent. All batch contact experiments were conducted using V/m = 80 mL g^{-1} in order to allow direct comparison of results. For the inactive Gd adsorption isotherm determinations, duplicate aliquots (5 mL) containing increasing concentrations of Gd (1−100 ppm) at a given concentration of HNO$_3$ (0.01M) were contacted with the given mesoporous phase (50 mg ± 1 mg) at 25 °C for 24 h with agitation. After this period the supernatant was removed, syringe filtered (0.45 μm), and the equilibrium metal cation concentrations analyzed determined using a Perkin-Elmer Elan 6000 inductively coupled plasma mass spectrometer (ICP-MS).

3. RESULTS AND DISCUSSION

Preparation of P-ZrTi-0.33 Adsorbent Phases.

Estimation of the level of functionalization was undertaken using simultaneous TGA-DTA analysis to determine the % mass loss due to the adsorbed organics in the temperature range ~200−600 °C. For an accurate determination of the starting point for combustion of the adsorbed organic molecules, drying of the functionalized phases to remove physisorbed water from the samples was required. The mass loss in the 30 − 200 °C range for the dried materials needed to be no more than 1.5% w/w for reproducible measurements. A similar approach was used by Mutin et al. (27), although the temperature range attributed to the loss of organics was considered to extend to higher temperatures than we have determined from our thermogravimetric analyses (~200−450 °C; see the Supporting Information, Figure S2).

The measured phosphonic acid loadings for the various functionalized ZrTi-0.33 phases are shown in Figure 3. The level of loading has been normalized relative to surface area of the mesoporous phase (m^2/g). The maximum level of functionalization (~3 molecules/nm^2) was observed for the simplest and smallest alkyl monophosphonic acid, **MeP**. This was lower than the 4.8 molecules/nm^2 observed by Mutin et al. for phenyl phosphonic acid and Degussa P25 powder (27). However, we have applied a more restrictive temperature range to the TGA-DTA data used to estimate the amount of organic present on the metal oxide phase. Moreover, these researchers performed their functionalization using nonaqueous solvents which may also give rise to some differences in loading. With increasing complexity of
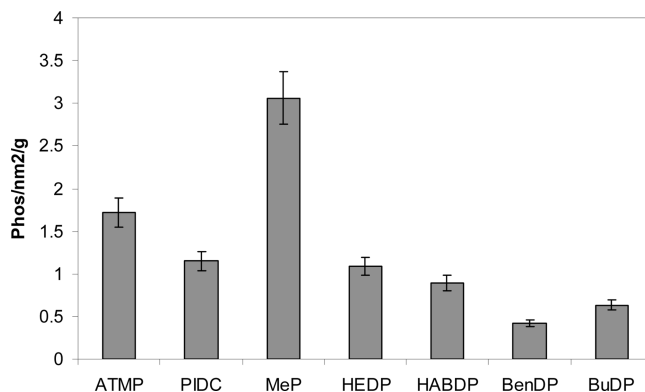

FIGURE 3. Degree of functionalization (molecules/nm^2) for the various phosphonic acids and the model ZrTi-0.33 framework. Error bars are nominally ~10% of the calculated functionalization level.

the phosphonic acid, the loading was observed to decrease by about 40% for the **ATMP** variant, 60% for the **PIDC**, **HEDP** and **HABDP** variants and 80% for the **BenDP** and **BuDP** variants. In all but the case of the **PIDC** molecule, coordination to the oxide surface was expected to occur through one or more of the available phosphonic acid groups. For the **PIDC** molecule, there was the possibility of coordination through the carboxylic acid groups. Nonetheless, the measured differences in loading appeared to be influenced by the potential mode of coordination to the surface. In contrast to **MeP**, which gave the highest surface loading, the lowest loadings were observed for **BenDP** and **BuDP**. In stretched configuration these are the longest of the molecules examined in this study and they could conceivably bind through each of the phosphonic acid end groups, especially within the curved surface of a pore. Hence, the relative size and structure of the individual phosphonic acids influenced the degree of functionalization.

It has been observed that the levels of functionalization were significantly lower than for pure titania in which less than a monolayer of coverage was observed. As an example, studies on the comparative binding of siloxanes and phosphonates to Ti-6Al-4 V alloy used in medical applications, propyl maleimido phosphonates were observed to not greatly influence surface loadings on this material (30).

Diffuse Reflectance FT-IR Spectroscopy (DRIFT).

DRIFT spectroscopic investigations of the hybrid **P-ZrTi-0.33** phases are presented in Figure 4. Also included for comparison is the spectrum of the parent model ZrTi-0.33 phase (Figure 4a). To better understand the coordination of the phosphonic acid in the hybrid phases, the background-corrected spectrum from each sample was decomposed to reveal the individual components of the observed spectrum in the region 1400−800 cm^{-1} (Figure 5). A summary of the DRIFT spectroscopy results is provided in Table 1.

The broad, unresolved bands at about 3300 cm^{-1} in each of the spectra have been attributed to hydrogen bonded, physi-sorbed water in the pores of the mesoporous phase. Even after extensive drying (10 mmHg, 100 °C), this broad envelope was consistently observed. As has been reported previously (22, 25, 27), infrared spectra of titanate and zirconate powders functionalized with phosphonic acids and
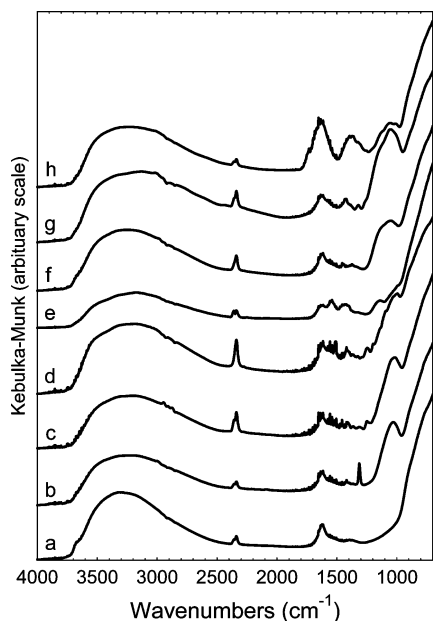
FIGURE 4. (a) DRIFT spectra of the parent mesoporous ZrTi-0.33 phase and (b–h) phosphonic acid functionalized phases in the region 4000–800 cm^{-1}. Legend: (b) MeP; (c) BuDP; (d) BenDP; (e) HABDP; (f) HEDP; (g) ATMP; (h) PIDC.
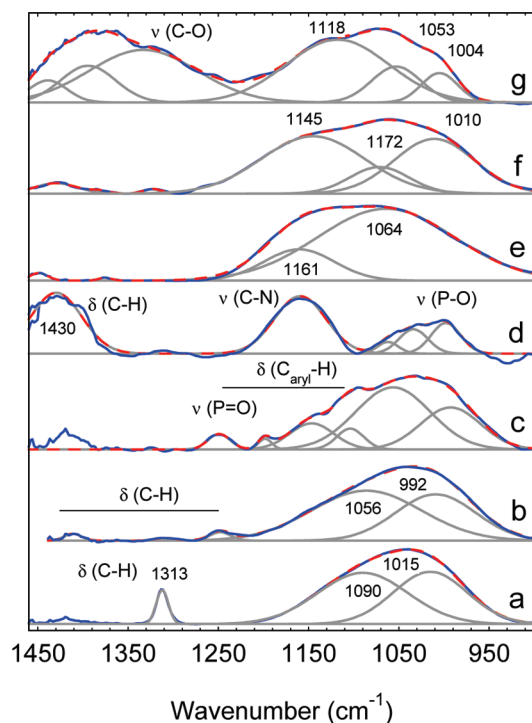

FIGURE 5. Decompositions of DRIFT spectra from functionalized mesoporous ZrTi-0.33 phases. Legend: (a) MeP; (b) BuDP; (c) BenDP; (d) HABDP; (e) HEDP; (f) ATMP; (g) PIDC.

phosphates usually contain a characteristically broad ν(P–O) band centered at about 1000 cm^{-1}. Given the potential for coordination to titanium and/or zirconium metal centers of the ZrTi-0.33 phase, further broadening of the ν(P–O) band was expected. Nonetheless, the spectra of the hybrid phases clearly show that each material contained coordinated phosphonic acid moieties.

For the simplest phosphonic acid, **MeP**, the spectral decomposition revealed two almost equal intensity compo-

nents that are assigned to the ν(P–O) bands of μ_3-coordinated phosphonic acid in a manner consistent with the literature (27). A sharp band at 1313 cm^{-1} that was also observed in the spectrum of the parent phosphonic acid has been assigned to the δ_s(C–H) deformation of the methyl group. The intensity and FWHM of this band suggested that the environment of the methyl group was extremely well-defined, implying rigid attachment to the oxide surface. The spectral decompositions suggested that the **BuDP**, **BenDP** molecules were primarily coordinated in a tridentate fashion to the oxide surface. Pawsey (25) and Guerrero (27) have previously commented on the range of ν(P–O) bands observed for phosphonic acids coordinated to the surface of titanate and zirconate powders. The shift to lower-frequency observed in the case of coordinated **BenDP** may or may not be indicative of a lower coordination number for the phosphonic headgroup. However, given that the ν(P=O) band at 1250 cm^{-1} continues to be observed for these two *bis*-phosphonates, it cannot be excluded on the basis of the FT-IR alone that one of the phosphonate groups remains at least partially unbound.

In the case of the 1,1-*bis*-phosphonic acids, **HEDP** and **HABDP**, the primary component identified from the spectral decompositions was positioned at about 1060 cm^{-1} with a lower intensity component at about 1160 cm^{-1}. In the case of the **HEDP** variant, the component at about 1060 cm^{-1} was extremely broad with an estimated fwhm of 176 cm^{-1}, suggesting that the coordination mode of the 1,1-*bis*-phosphonic acid anchor group was highly variable. Moreover, given the broadness of the 1060 cm^{-1} band, it is probable that there exists a contribution from [P]–OH moieties. This could result from either bidentate or loosely bound phosphonic acid groups. The observed variable coordination is consistent with a previous investigation of the binding of **HEDP** to hydroxyapatite surfaces (31). In the case of the **HABDP** variant, however, the bands indicative of coordinated phosphonic acid were well-defined and similar to those observed for **MeP**-, **BuDP**-, and **BenDP**-ZrTi-0.33. Other bands associated with the amine and alkyl chain can be observed in the spectrum of an extended spectral region for the HABDP variant (see the Supporting Information, Figure S2). It is also notable that the ν(P=O) band is absent for these two 1,1,-*bis*-phosphonates, suggesting that both phosphonic acid groups are bound, even if only in a bidentate fashion.

Decomposition of the DRIFT spectrum of **ATMP**-ZrTi-0.33 indicated three principal components (Figure 5f). Two of the components were assigned to tridentate or strongly coordinated phosphonic acid groups. In comparison with the spectrum of the parent **ATMP** and 1,1-*bis*-phosphonic acid variants, the component at 1145 cm^{-1} appeared to be due to phosphonic acid groups that were only loosely bound to the oxide surface. The decomposition suggested that these groups were present in a 0.65: 1 ratio with strongly coordinated groups. The broad nature of the spectral envelope and its overlap with the region of ν(P=O) vibration suggests the

Table 1. FTIR Band Assignments for the Various Phosphonic Acids

[P]-ZrTi-0.33 Phase	R-PO$_3$ (cm^{-1})	other (cm^{-1})		assignment
BuDP	1086, 1009	3050−2900	C−H stretch	
		1400−1200	CH$_2$ in/out-of-plane deformation	
BenDP	1056, 992	3050−2900	C−H (alkyl/aryl) stretch	
		1400−1100	ring stretch, C−H out-of-plane	
HABDP	1061, 1034, 998	3050−2900	C−H stretch	
		1660−1150	C−N stretch, CH$_2$ in/out-of-plane deformation, N−H bend	
HEDP	1160, 1064	3050−2900	C−H stretch	
ATMP	1145, 1072, 1010	3050−2900	C−H stretch	
PIDC	1118, 1054, 1004	3050−2900	C−H stretch	
		1600, 1400	C−O bridging carboxylate	

possibility of one free phosphonic group for some of the coordinated molecules.

Decomposition of the **PIDC**-ZrTi spectrum in the 1500−800 cm^{-1} region (Figure 5g) revealed three components due to coordination of phosphonic acid groups. A broad band at about 1400 cm^{-1} (and 1600 cm^{-1} not shown) appeared characteristic of the ν(C−O) vibration from coordinated bridging carboxylate groups (11, 16, 25) (Figure 4h). There was no indication of the presence of free carboxylic acid groups (formally R-CO$_2$H). On the basis of the spectra for the other hybrid phases, the two lowest wavenumber bands appeared to correspond to phosphonic acid strongly coordinated to the oxide surface. Furthermore, these species appeared to be present in a significantly lower proportion than the component centered at higher wavenumber (1118 cm^{-1}), which corresponds to phosphonic acid only weakly bound to the oxide surface. The implications of this variable coordination will be discussed further in the ^{31}P MAS NMR and ion-exchange sections below.

^{31}P MAS NMR Spectroscopy. From the results of the DRIFT spectroscopy, qualitative differences in the coordination of the different phosphonic acids were apparent. In an attempt to corroborate the DRIFT results, simple Bloch decay and cross-polarized (CP) ^{31}P MAS NMR studies were performed on the parent phosphonic acids and the series of hybrid phases (Figure 6). In each spectrum, a large degree of chemical shift dispersion was evident for the observed resonances and this was consistent with the observations from the DRIFT spectroscopy. Examination of an extended chemical shift range to that presented in Figure 6 revealed that the resonances of each spectrum displayed some chemical shift anisotropy (CSA), which was unable to be averaged by the MAS frequency of ∼10 kHz. Decomposition of the ^{31}P NMR spectra was undertaken with the results presented graphically in Figure 7.

The ^{31}P NMR spectra of the **MeP-**, **BuDP-**, and **BenDP-** containing phases all consisted of essentially a single broad component with a shift between about 5−12 ppm upfield of the narrow chemical shift for the corresponding free phosphonic acid. This was entirely consistent with coordination of the phosphonic acid groups to a metal oxide surface via a similar binding mode. The broadness of the resonances and the lack of discernible structure in the ^{31}P MAS NMR spectra was similar to that observed for *bis*-phosphonates anchored to bone where the replacement of phosphate

groups belonging to the calcium phosphate phase and interaction with calcium sites effectively reduced or eliminated motional averaging (32). An important difference between the ^{31}P MAS NMR spectra observed here and the spectra observed by Guerrero et al. (33) for phenylphosphonic acid-grafted TiO$_2$ (Degussa P25) is that in the present case there is only a single resonance that is substantially broad-
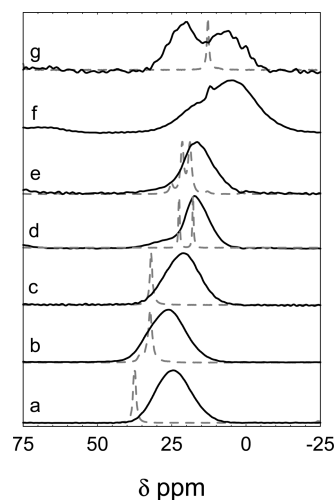

FIGURE 6. ^{31}P MAS NMR spectra of free phosphonic acids (---) and phosphonic acid functionalized ZrTi-0.33 phases. (a) MeP; (b) BuDP; (c) BenDP; (d) HABDP; (e) HEDP; (f) ATMP; (g) PIDC.
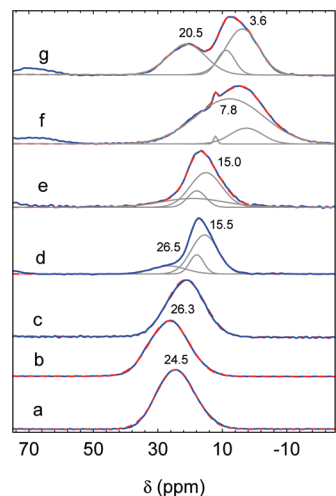

FIGURE 7. Spectral decompositions of ^{31}P MAS NMR spectra of functionalized mesoporous ZrTi-0.33 phases. (a) MeP; (b) BuDP; (c) BenDP; (d) HABDP; (e) HEDP; (f) ATMP; (g) PIDC.

ened, compared to the multiple resonances observed by these authors.

It is important to emphasize that the observation of only a single resonance suggests a single, probably tridentate, binding mode and that this is broadly consistent with the infrared spectroscopy. In the case of both **BuDP** and **BenDP** that have rather long alkyl or phenyl spacers, it is possible to envisage binding of both end groups to the metal oxide surfaces. Regarding the spectral linewidths, Pawsey et al. (34) have shown that broader resonances are usually observed for *bis*-phosphonates bound to ZrO_2 because of the stronger binding that occurs with ZrO_2 surfaces. This suggests that in the present mesoporous mixed oxides binding of the phosphonates to surface zirconium sites occurs in preference to titanium.

In contrast to the alkyl and phenyl phosphonic acids (**MeP**, **BuDP**, and **BenDP**), the spectra of the **HABDP**-, **HEDP**-, **ATMP**-, and **PIDC**-ZrTi-0.33 were more complex. Each spectrum contained resonances shifted upfield by a similar magnitude to the other phases, thus supporting the results from the infrared spectroscopy. A graphical comparison of the upfield shift observed for the resonances of free and coordinated phosphonic acid group for the most part emphasizes the shift difference and bears out the assertion that each of the phosphonic acid molecules is able to bind strongly with the oxide surface (see the Supporting Information, Figure S3). The variable coordination modes indicated by the infrared spectroscopy for the **HABDP**, **HEDP**, **ATMP**, and **PIDC** molecules are clearly evident as judged from the shallower sloped plots of each. In the case of the **ATMP** and **PIDC** variants, the components attributable to the shallower plots accounted for >50 % of the total intensity of the spectral envelope. Additionally, the decomposition of the **PIDC** and **ATMP** variant spectra both contained components that were downfield of the resonance for the corresponding free acid (about 37 and 17 %, respectively).

In the case of **PIDC**, several options exist for binding of this molecule to the zirconium titanate surface. In the case of carboxyalkylphosphonic acids, $HO_2C(CH_2)_nPO_3H_2$ ($n = 2$, 3, 11, and 15), it has been shown that selective binding occurs via the phosphonate group (25). The spectral envelop of the **PIDC** hybrid was significantly broadened. Decomposition into three broad components was possible, suggesting that the phosphonate group has multiple binding modes to the oxide surface.

Considering next the 1,1-*bis*-phosphonic acid variants, **HABDP** and **HEDP**, the general downfield shift of the spectral envelop relative to the respective free acids (Figure 6) was suggestive of strong binding to the oxide surface. The doublet structure of **HEDP** and **HABDP** salts observed in Figure 6 was consistent with the noncentrosymmetric crystal structures for these compounds (35). The ^{31}P resonances were significantly broadened compared with those of the free phosphonic acids suggesting similar chemical binding of the *bis*-phosphonates as the alkyl and aryl phosphonates. If only physi-sorption were involved, then much narrower ^{31}P resonances would have been expected. Indeed, the

recently reported MAS NMR spectra of **HEDP**-TiO_2 hybrids contained one or more ^{31}P chemical shifts near 16 ppm (36, 37) that is close to the shift observed for the center of the spectral envelope of the **HEDP**-ZrTi-0.33 hybrid. As the central envelope of the ^{31}P NMR spectra of these two hybrids comprised multiple components, this suggests that different binding modes are possible for the individual phosphate groups.

In the case of **ATMP**, which is a hygroscopic liquid, the chemical shift of pure **ATMP** under MAS conditions was acquired by doping solid **ATMP**-ZrTi-0.33 with pure **ATMP** (0.1 % w/w) and then comparing with an undoped sample. Using this approach, the sharp resonance at about 12 ppm in the spectrum of **ATMP**-ZrTi-0.33 was assigned to free phosphonic acid groups. The ^{31}P MAS NMR results for the **ATMP** hybrid seemingly indicated the presence of a small amount of uncoordinated free phosphonic acid groups and a significant level of weakly coordinated phosphonic acid groups, and thus are in reasonable agreement with the infrared spectroscopy. The presence of free phosphonic acid groups is presumably responsible for the binding of solution metal species by this hybrid, as will be further discussed below.

Summarizing the spectroscopic results it is possible to conclude that **MeP** exhibits complete tridentate coordination to the zirconium titanate surface because there is no ν(P=O) band observed in the DRIFT and the NMR shows only a single broad resonance. For the two linear *bis*-phosphonates, **BuDP** and **BenDP**, some bidentate character can be postulated on the basis of the presence of the ν(P=O) band, whereas it is impossible to completely rule out the existence of a small proportion of free phosphonate groups from the broad NMR. For the two 1,1-*bis*-phosphonates, **HABDP** and **HEDP**, the binding mode appears to be variable but no free phosphonate was detected by NMR. In the case of **ATMP**, NMR suggests the existence of some free phosphonate, whereas FT-IR cannot totally exclude the possibility of some bidentate character. The binding mode of **PIDC** seems to be consistent with the other two 1,1-*bis*-phosphonates.

Ion Exchange Properties: Affinity for ^{153}Gd Radiotracer. The importance of radio-lanthanide and minor actinide removal from current irradiated nuclear reprocessing waste streams stems largely from a need to manage radioactivity responsibly. However, in advanced fuel cycles where efficient minor actinide recovery and management is crucial, separation of bulk and trace levels of radio-lanthanides from minor actinide-rich processing streams poses a significant challenge. Following the characterization of the hybrid phases, the adsorption of lanthanide cations from acidic solution was explored. The affinity for carrier-free ^{153}Gd radiotracer was determined across a range of nitric acid concentrations (0.00001−3.0 M). The distribution coefficients (mL/g) for all samples at selected acid concentrations of 0.01, 0.001, and 0.00001 are shown in Figure 8. The kinetics of ^{153}Gd adsorption was explored at an intermediate acid concentration (0.01 M) for each phase. This demonstrated that contact times of less
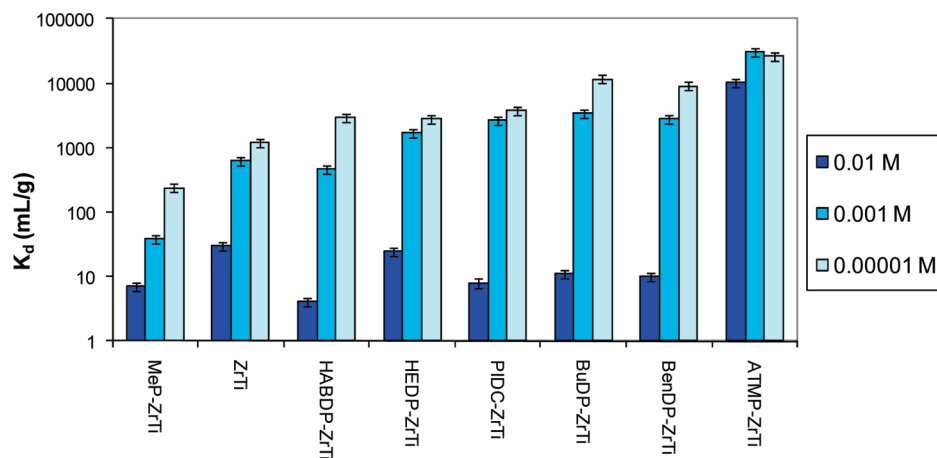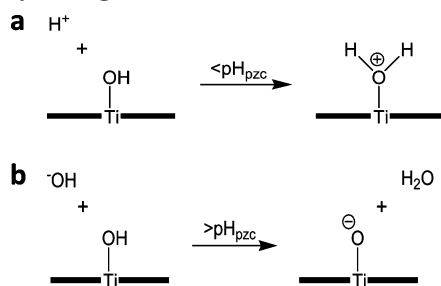
FIGURE 8. Carrier-free ^{153}Gd distribution coefficients (mL/g) measured for unfunctionalized ZrTi-0.33 and P-ZrTi-0.33 where P represents a range of phosphonates measured across a wide range of nitric acid concentrations (0.00001−0.01 M).

Scheme 2. (a) Protonation and (b) Deprotonation of a Metal Oxide Surface Leading to a Positively or Negatively Charged Surface

than 30 min were sufficient for maximum adsorption. Preliminary investigations of the hydrolytic stability of these phases under similarly acidic conditions for extended contact times (≤72 h) have shown that the contact times used in this study, resulted in <0.1 % of coordinated phosphonic acid released to solution. These hydrolytic stability data are part of a more comprehensive study which will be communicated in the near future.

Unlike traditional polymeric ion exchange resins, the adsorption of cations and/or anions by the metal oxide framework of these hybrid adsorbents must be considered. In other words, those regions of the pore surfaces that do not contain functional molecules and that are capable of binding metal ion species. This adsorption phenomenon is dependent on the point of zero charge (pH$_{pzc}$), which is intimately linked to the pH of the aqueous solution in contact with the given metal oxide. In the case of the mixed zirconium−titanium oxide framework being considered here, values of about 5 have been measured (see the Supporting Information, Figure S4). As the pH of solution is lowered, protonation of the surface (hydroxyls) according to Scheme 2a becomes more prevalent and the surface bears a net positive charge. When the pH is raised above the pH$_{pzc}$, then deprotonation of the surface (hydroxyls) occurs according to Scheme 2b and the surface bears a net negative charge. In this communication, we will refer to adsorption by the metal oxide framework as "nonselective".

In the case of titanate and zirconate phases, it is well-known that these oxides display affinity for cations and

anions across a wide pH range with the mechanisms of adsorption varying from simple electrostatic attraction to surface complexation and ligand exchange (38−41). Hence, quantification of this behavior for the hybrid phases and ^{153}Gd^{3+} adsorption across the acid concentration range of interest was crucial to the interpretation of the ion exchange results. In the plot of Figure 8, the "nonselective" adsorption of ^{153}Gd^{3+} by the unfunctionalized mesoporous ZrTi-0.33 can be seen to have been significant at acid concentrations of 0.00001 and 0.001 M (K_d = 1192 and 628 mL/g, respectively (≈90 % extraction). The uptake of ^{153}Gd^{3+} decreased significantly at higher concentrations of acid and was negligible at >0.1 M. In a previous communication (12), the pH$_{pzc}$ of the ZrTi-0.33 framework was reported to be 4.8 ± 0.1, so the adsorption behavior for ^{153}Gd^{3+} observed here was as expected.

Lanthanides are classified as hard acids and as such prefer hard bases which is how all of the binding groups of the molecules investigated here can be classified. However, it is well-known that phosphonic acids display a strong affinity for actinides and lanthanides (42−45). Indeed this is born out in the plot of Figure 8 with the **MeP**- ZrTi-0.33 phase (no potential free phosphonic groups) exhibiting the lowest affinity for ^{153}Gd and **ATMP**- ZrTi-0.33 that was concluded to have at least some free phosphonic acid groups exhibiting the highest.

Given that a proportion of the pore surface area of each hybrid phase is occupied by grafted phosphonic acid molecules, the adsorption measured for the parent ZrTi-0.33 phase probably represents an overestimation of the level of "nonselective" adsorption. The decrease in ^{153}Gd^{3+} affinity through a decrease in available surface area should be able to be demonstrated using the **MeP**-functionalized phase. The plot of ^{153}Gd adsorption for the **MeP**-ZrTi-0.33 phase in Figure 8 supports this with a decrease in the ^{153}Gd distribution coefficients across the entire acid concentration range studied. Therefore, the parent ZrTi-0.33 and **MeP**-ZrTi-0.33 phases represent the two extremes possible with respect to the "nonselective" adsorption of ^{153}Gd^{3+} on the oxide surface. Importantly, these results show that although at intermediate to low acid concentrations "nonselective" adsorp-

tion is a consideration, at acid concentrations of >0.1 M, "nonselective" adsorption is unlikely and can be neglected. Although we have not specifically elucidated the mechanism of $^{153}Gd^{3+}$ adsorption at low acid concentrations, given that hydrolysis of $[Gd(H_2O)_x]^{3+}$ normally occurs above about pH 6 (46), "nonselective" adsorption probably involves adsorption/surface complexation of the simple hydrated cation (47).

The summary of the $^{153}Gd^{3+}$ binding data for unfunctionalized and a majority of the functionalized ZrTi-0.33 phases was that at >0.01 M HNO_3, there was little tendency for gadolinium binding. At $[H^+]$ >0.01 M, "nonselective" adsorption of $^{153}Gd^{3+}$ by the **MeP**-ZrTi-0.33 phase was the lowest of all the samples ($K_d = 7 \pm 1$ mL/g) with the **HABDP**-, **PIDC**-, **BuDP**-, and **BenDP**-functionalized variants also displaying relatively low affinity for $^{153}Gd^{3+}$ at this acid concentration. This adsorption behavior indicated that the phosphonic acid groups in each of these hybrid phases were either strongly coordinated to the pore surface, or were relatively constrained such that there were no phosphonic acid groups available to coordinate $^{153}Gd^{3+}$. For the **BuDP** and **BenDP** variants, these observations supported the results of the spectroscopic studies. For the **HABDP**-, **HEDP**-, and **PIDC**-ZrTi-0.33 phases, however, where the coordination to the pore surface was tridentate and for which no free phosphonate was identified, the binding of ^{153}Gd also appeared to be relatively nonselective at high acid concentration.
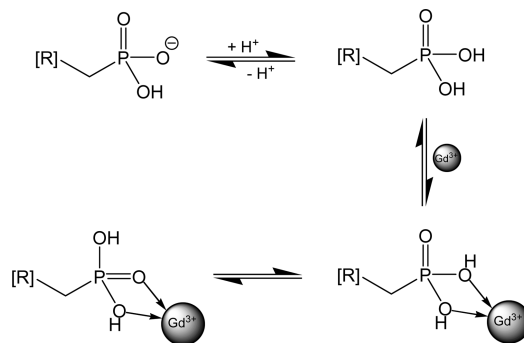
For the **ATMP**-ZrTi-0.33 phase, the affinity for ^{153}Gd tracer was significantly higher than that displayed by the other hybrid phases especially at 0.01 M HNO_3. The measured ^{153}Gd K_d of 10145 $\pm$ 857 mL/g at this acid concentration demonstrated that the coordinated **ATMP** molecule was able to impart sufficient affinity to extract a significant proportion of the ^{153}Gd radiotracer (>99%). Regardless of whether the level of "nonselective" adsorption was defined with respect to the ZrTi-0.33 or the **MeP**-ZrTi-0.33 phase, the level of extraction that could be unequivocally attributed to the coordinated **ATMP** molecule was >74% (74−91%).

The pK_a of alkyl amino-phosphonic acids in aqueous solutions are well-known to occur at about pH 6.0 and 2.0 (48, 49). Hence, for a majority of the acid concentration range studied here, any "free" phosphonic acid group (of an **ATMP** molecule) should exist as the monoanion with a small proportion of the dianion at higher pH. The high affinity of the **ATMP**-ZrTi-0.33 hybrid for ^{153}Gd in the range pH 6 - 3 can therefore be attributed to a combination of "nonselective" adsorption, and coordination by deprotonated phosphonic acid groups (Scheme 3). At lower pH (>0.01 M HNO_3), protonation is favored, thereby affording the neutral phosphonic acid, which from the adsorption experiments also conferred a degree of affinity for ^{153}Gd (Scheme 4). Given the observed sustained affinity under these acidic conditions, it is possible to hypothesize that deprotonation of the phosphonic acid group is not essential for coordination of ^{153}Gd. Although such a hypothesis seems reasonable, the question can be posed as to why the other **P**-ZrTi-0.33 hybrid phases with loosely coordinated phosphonic acid groups did

Scheme 3. Coordination of $^{153}Gd^{3+}$ by Deprotonated Phosphonic Acid Groups As Determined by the pH of the Aqueous Solution
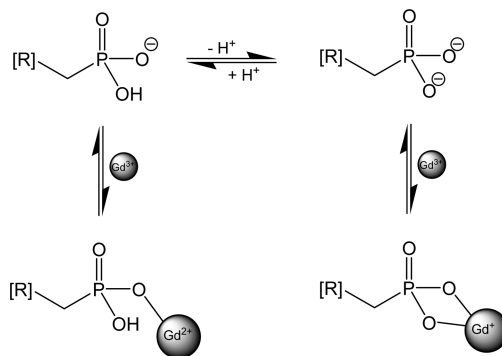
Scheme 4. Coordination of $^{153}Gd^{3+}$ by Protonated Phosphonic Acid Groups at pH Values below the pKa

not also display some affinity for ^{153}Gd under similar conditions? Reconsidering the decomposition of the ^{31}P MAS NMR spectrum for the **ATMP**-ZrTi-0.33 hybrid phase, the presence of strongly coordinated phosphonic acid groups was assured by the observation of a component at about 2 ppm, which was about 10 ppm upfield of the free **ATMP** acid. This component only corresponded to about 14% of the total integrated intensity with the remaining intensity from a broad component at about 8 ppm, which was assigned to loosely coordinated phosphonic acid groups. The loosely coordinated phosphonic acid groups of the surface bound **ATMP** ligand should be able to act as a chelating agent for ^{153}Gd (Figure 9).

The affinity of the **ATMP**-ZrTi-0.33 hybrid phase for Gd^{3+} was also observed at macro-concentrations and 0.01 M HNO_3 (Figure 10). The adsorption isotherm for the parent
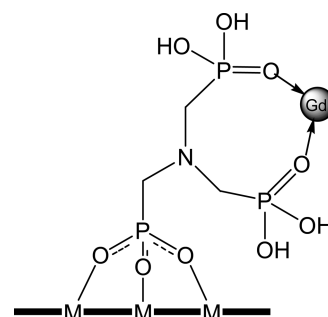

FIGURE 9. Hypothesized chelation model explaining the affinity of ATMP-ZrTi-0.33 for ^{153}Gd at low pH.
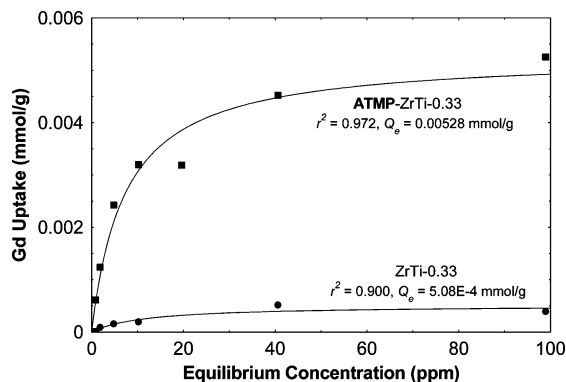
FIGURE 10. Equilibrium isotherm plots for ZrTi-0.33 and ATMP-ZrTi-0.33, and the adsorption of Gd from 0.01 M HNO3. $V/m = 100$ mL/g and 24 h contact time.

ZrTi-0.33 phase was also determined under similar conditions. Both isotherms were successfully modeled using the standard Langmuir isotherm. Significantly inferior fits were experienced using the Freundlich model ($r^2 < 0.8$) which suggested that the materials had a well-defined adsorption capacity for Gd, and that there was a relatively consistent adsorption mechanism at play under these conditions. The calculated theoretical uptake for Gd of about 0.00051 mmol/g for the parent ZrTi-0.33 phase was an order of magnitude lower that of the **ATMP**-ZrTi-0.33 hybrid phase. This again highlights the point that although "nonselective" adsorption decreases markedly with increasing HNO$_3$ concentration, the level of "nonselective" adsorption is an important factor in determining the overall affinity of these types of hybrid materials at intermediate to low pH.

The adsorption capacity for **ATMP**-ZrTi-0.33 determined from the adsorption isotherm is low in comparison with traditional organic ion exchange resins. This study focused on the functionalization of a mesoporous zirconium titanate post synthesis after removal of the template by calcination. This approach was adopted in order to preserve the structural and textural properties of the mesoporous framework, and to ensure that these properties would not be significantly altered by phosphonic acid functionalization. However, the approach suffers from the generally low level of functionalization that can be achieved since functionalization depends on hydroxyl group density, which is expected to be relatively low for the calcined framework. Moreover, calcination also lowers the level of coordinative unsaturation of the surface which is another potential mode for coordination. Future work to develop commercially viable materials would need to address increasing the capacity of the hybrids. Of course, other approaches such as low-temperature removal of the templating molecules and the introduction of the functional units during initial synthesis also need to be considered.

4. CONCLUSIONS

The functionalization of mesoporous zirconium titanate xerogel powders with a number of commercial and readily synthesized mono-, bis-, and tris-phosphonic acids has been studied. The stability and strength of the M−O−P linkage makes the use of phosphonic acid anchor groups a simple and effective approach to functionalizing the internal oxide surface and producing a new range of hybrid inorganic−organic materials. For the phosphonic acids employed in this study, the level of surface functionalization (molecules/nm^2) is primarily related to the potential coordination mode of the parent acid molecule to the oxide surface and not the molecular dimensions. This is because functionalization occurs well below that expected for complete monolayer coverage. Both DRIFT and ^{31}P MAS NMR spectroscopy of the functionalized phases clearly shows that the phosphonic acid molecules can coordinate strongly to the metal oxide surface. Nonetheless, the coordination can be highly variable, especially in the case of polyphosphonic acids such as ATMP, where the existence of some free phosphonate groups appears most probable.

Radiotracer studies with ^{153}Gd have highlighted that the presence of loosely coordinated (bidentate) phosphonic acid groups does not automatically translate to affinity for lanthanide cations. Any assessment of the adsorption properties for metal cations by these hybrid phases at acid concentrations of <0.1 M must take into account the "nonselective" adsorption by the oxide framework. For the mesoporous phase functionalized with amino *tris*-methylenephosphonic acid molecules (**ATMP**-ZrTi-0.33), surprisingly high affinity for ^{153}Gd across a wide range of H$_3$O$^+$ concentrations has been observed. The absence of similar behavior by the other hybrid materials containing loosely coordinated phosphonic acid groups appears to suggest that the affinity for ^{153}Gd is likely to be attributable to the availability of unbound or partially bound phosphonic acid groups. Hence, the surface bound **ATMP** ligand functions as a chelating ligand toward ^{153}Gd. Further studies of the affinity of the **ATMP**-ZrTi-0.33 hybrid phase for ^{153}Gd and the minor actinide, ^{241}Am, in the presence of varying levels of competing cations has commenced and will be reported in due course.

Supporting Information Available: The thermogravimetric data for **ATMP**-ZrTi-0.33, spectral decomposition of the DRIFT spectrum of the **HABDP**-ZrTi-0.33 material in the 1700−800 cm^{-1} region, and zeta potential measurement plot for ZrTi-0.33 (PDF). This material is available free of charge via the Internet at http://pubs.acs.org.

REFERENCES AND NOTES

(1) Hoffmann, F.; Cornelius, M.; Morell, J.; Froba, M. *Angew. Chem., Int. Ed.* **2006**, *45*, 3216.
(2) Fryxell, G. E. *Inorg. Chem. Commun.* **2006**, *9*, 1141.
(3) Fryxell, G. E.; Liu, J. *Designing Surface Chemistry in Mesoporous Silica*; Marcel Dekker: New York, 2000.
(4) Moller, K.; Bein, T. *Chem. Mater.* **1998**, *10*, 2950.
(5) Stein, A.; Melde, B. J.; Schroden, R. C. *Adv. Mater.* **2000**, *12*, 1403.
(6) Kimura, T. *Chem. Mater.* **2005**, *17*, 337.
(7) Athens, G. L.; Shayib, R. M.; Chmelka, B. F. *Curr. Opin. Colloid Interface Sci.* **2009**, *14*, 281.
(8) Zhang, X.-J.; Ma, T.-Y.; Yuan, Z.-Y. *J. Mater. Chem.* **2008**, *18*, 2003.
(9) Fryxell, G. E.; Wu, H.; Lin, Y.; Shaw, W. J.; Birnbaum, J. C.; Lineham, J. C.; Nie, Z.; Kemner, K.; Kelly, S. *J. Mater. Chem.* **2004**, *14*, 3356.
(10) Etienne, M.; Walcarius, A. *Talanta* **2003**, *59*, 1173.
(11) Luca, V.; Bertram, W.; Widjaja, J.; Mitchell, D. R. G.; Griffith, C. S.; Drabarek, E. *Microporous Mesoporous Mater.* **2007**, *103*, 123.
(12) Griffith, C. S.; Sizgek, G. D.; Sizgek, E.; Scales, N.; Yee, P. J.; Luca, V. *Langmuir* **2008**, *24*, 12312.

(13) Sizgek, G. D.; Sizgek, E.; Griffith, C. S.; Luca, V. *Langmuir* **2008**, *24*, 12323.

(14) Clearfield, A. *Prog. Inorg. Chem.* **1998**, *47*, 371.

(15) Park, H.; Bae, E.; Lee, J.-J.; Park, J.; Choi, W. *J. Phys. Chem. B* **2006**, *110*, 8740.

(16) Bae, E.; Choi, W.; Park, J.; Shin, H. S.; Kim, S. B.; Lee, J. S. *J. Phys. Chem. B* **2004**, *108*, 14093.

(17) Yan, S. G.; Hupp, J. T. *J. Phys. Chem.* **1996**, *100*, 6867.

(18) Pechy, P.; Rotzinger, F. P.; Nazeruddin, M. K.; Kohle, O.; Zaker-uddin, S. M.; Humphy-Baker, R.; Gratzel, M. *J. Chem. Soc., Chem. Commun.* **1995**, 65.

(19) Lee, H.; Kepley, L. J.; Hong, H.-G.; Mallouk, T. E. *J. Am. Chem. Soc.* **1988**, *110*, 618.

(20) Putvinski, T. M.; Schilling, M. L.; Katz, H. E.; Chidsey, C. E. D.; Mujsce, A. M.; Emerson, A. B. *Langmuir* **1990**, *6*, 1567.

(21) Gardner, T. J.; Frisbie, C. D.; Wrighton, M. S. *J. Am. Chem. Soc.* **1995**, *117*, 6927.

(22) Gawalt, E. S.; Avaltroni, M. J.; Koch, N.; Schwartz, J. *Langmuir* **2001**, *17*, 5736.

(23) Danahy, M. P.; Avaltroni, M. J.; Midwood, K. S.; Schwarzbauer, J. E.; Schwartz, J. *Langmuir* **2004**, *20*, 5333.

(24) Hofer, R.; Textor, M.; Spencer, N. D. *Langmuir* **2001**, *17*, 4014.

(25) Pawsey, S.; Yach, K.; Reven, L. *Langmuir* **2002**, *18*, 5205.

(26) Fadeev, A. Y.; Helmy, R. *Langmuir* **2002**, *18*, 8924.

(27) Guerrero, G.; Mutin, P. H.; Vioux, A. *Chem. Mater.* **2001**, *13*, 4367.

(28) Lafond, V.; Gervais, C.; Maquet, J.; Prochnow, D.; Babonneau, F.; Mutin, P. H. *Chem. Mater.* **2003**, *15*, 4098.

(29) Danahy, M. P.; Avaltroni, M. J.; Midwood, K. S.; Schwarzbauer, J. E.; Schwartz, J. *Langmuir* **2004**, *20*, 5333.

(30) Silverman, B. M.; Wieghaus, K. A.; Schwartz, J. *Langmuir* **2005**, *21*, 225.

(31) Cukrowski, I.; Popovic, L.; Barnard, W.; Paul, S. O.; Van Rooyen, P. H.; Liles, D. C. *Bone* **2007**, *41*, 668.

(32) Mukherjee, S.; Song, Y.; Oldfield, E. *J. Am. Chem. Soc.* **2008**, *130*, 1264.

(33) Guerrero, G.; Mutin, P. H.; Vioux, A. *Chem. Mater.* **2000**, *12*, 1268.

(34) Pawsey, S.; Mccormick, M.; De Paul, S.; Graf, R.; Lee, Y. S.; Reven, L.; Spiess, H. W. *J. Am. Chem. Soc.* **2003**, *125*, 4174.

(35) Grossmann, G.; Grossmann, A.; Ohms, G.; Breuer, E.; Chen, R.; Golomb, C.; Cohen, H.; Hagele, G.; Classen, R. *Magn. Reson. Chem.* **2000**, *38*, 11.

(36) Zhang, X.-J.; Ma, T.-Y.; Yuan, Z.-Y. *Eur. J. Inorg. Chem.* **2008**, 2721.

(37) Ma, T.-Y.; Zhang, X.-J.; Shao, G.-S.; Cao, J.-L.; Yuan, Z.-Y. *J. Phys. Chem. C* **2008**, *112*, 3090.

(38) Khalil, T.; El-Sweify, F. H.; El-Gammal, B.; El-Nour, F. A. *J. Radioanal. Nucl. Chem.* **1997**, *222*, 61.

(39) Gurboga, G.; Tel, H.; Altas, Y. *Sep. Purif. Technol.* **2006**, *47*, 96.

(40) Abe, M. *Inorg. Ion Exch. Mater.;* **1982**, 161–273.

(41) Yinjie, S.; Liqiang, J.; Aimin, Z.; Qixin, J.; Dakang, S. *J. Radioanal. Nucl. Chem.* **1997**, *222*, 75.

(42) Mathur, J. N.; Murali, M. S.; Nash, K. L. *Solvent Extr. Ion Exch.* **2001**, *19*, 357.

(43) Nash, K. L.; Jensen, M. P.; Schmidt, M. A. *J. Alloys Compd.* **1998**, *271–273*, 257.

(44) Nash, K. L. *J. Alloys Compd.* **1997**, *249*, 33.

(45) Chiarizia, R.; Barrans, R. E.; Ferraro, J. R.; Herlinger, A. W.; Mcalister, D. R. *Sep. Sci. Technol.* **2001**, *36*, 687.

(46) Baes, C. F. J.; Mesmer, R. E. *The Hydrolysis of Cations*; Krieger Publishing Company: Malabar, FL, 1986.

(47) Bourikas, K.; Hiemstra, T.; Van Riemsdijk, W. H. *Langmuir* **2001**, *17*, 749.

(48) Franz, R. G. *AAPS Pharmsci.* **2001**, *3* (2), article 10.

(49) Jencks, W. P.; Westheimer, F. H. 2003. Aqueous pKa Values. Web Page, http://jce.divched.org/JCEDLib/, accessed 2008.

AM100891U